

Alma Mater Studiorum Università di Bologna
Archivio istituzionale della ricerca

Theoretical Study on the Optoelectronic Properties of Merocyanine- Dyes

This is the final peer-reviewed author's accepted manuscript (postprint) of the following publication:

Published Version:

Ritu Tomar, L.B. (2023). Theoretical Study on the Optoelectronic Properties of Merocyanine- Dyes. JOURNAL OF PHYSICAL CHEMISTRY. A, MOLECULES, SPECTROSCOPY, KINETICS, ENVIRONMENT, & GENERAL THEORY, 127, 9661-9671 [10.1021/acs.jpca.3c04226].

Availability:

This version is available at: <https://hdl.handle.net/11585/954257> since: 2024-02-19

Published:

DOI: <http://doi.org/10.1021/acs.jpca.3c04226>

Terms of use:

Some rights reserved. The terms and conditions for the reuse of this version of the manuscript are specified in the publishing policy. For all terms of use and more information see the publisher's website.

This item was downloaded from IRIS Università di Bologna (<https://cris.unibo.it/>).
When citing, please refer to the published version.

(Article begins on next page)

This is the final peer-reviewed accepted manuscript of:

J. Phys. Chem. A 2023, 127, 9661–9671

The final published version is available online at:

<https://doi.org/10.1021/acs.jpca.3c04226>

Terms of use:

Some rights reserved. The terms and conditions for the reuse of this version of the manuscript are specified in the publishing policy. For all terms of use and more information see the publisher's website.

This item was downloaded from IRIS Università di Bologna (<https://cris.unibo.it/>)

When citing, please refer to the published version.

A Theoretical Study on the Optoelectronic Properties of Merocyanine-Dyes

Ritu Tomar,[†] Leonardo Bernasconi,[‡] Daniele Fazzi,[¶] and Thomas Bredow^{*,†}

[†]*Mulliken Center for Theoretical Chemistry, Clausius-Institut für Physikalische und
Theoretische Chemie, Universität Bonn, Beringstraße 4, 53115 Bonn, Germany*

[‡]*Center for Research Computing and Department of Chemistry, University of Pittsburgh,
USA*

[¶]*Dipartimento di Chimica "Giacomo Ciamician", Università di Bologna, via F. Selmi 2,
Bologna, Italy*

E-mail: bredow@thch.uni-bonn.de

Phone: +49 (0)228 733839

Abstract

Merocyanines, as prototypes of highly polar π -conjugated molecules, have been intensively investigated for their self-assembly and optoelectronic properties, both experimentally and theoretically. However, an accurate description of their structural and electronic properties remains challenging for quantum-chemical methods. We assessed several theoretical approaches, TD-DFT, GW-BSE, STEOM-DLPNO-CCSD, and CASSCF/NEVPT2-FIC for their reliability to reproduce optoelectronic properties of a series of donor/acceptor (D/A) merocyanines, focusing on the first excitation energy. Additionally, we tested an all-electron perturbative method based on time-dependent coupled-perturbed density functional theory, denoted as TDCP-DFT. Particular focus was set on direct and indirect solvent effects which affect excited-state energies by electrostatic interaction and molecular geometry. The molecular configuration space was sampled at the semiempirical tight-binding level. Our results corroborate previous investigations, showing that the S_0 - S_1 excitation energy strongly depends on the merocyanine molecular structure and the dielectric constant of the solvent. We found significant effects of the polar solution environment on the geometry of the merocyanines, which strongly affects the calculated excitation energies. Taking these effects into account best agreement between calculated and measured excitation energies was obtained with TDCP-DFT and GW-BSE. We also calculated excitation energies of molecular crystals at TDCP-DFT level, and compared the results to the corresponding monomers.

Introduction

Merocyanines (MCs) are excellent candidates for optoelectronic applications because their optical properties can be easily tailored using chemical and physical methods. MCs have been intensively investigated, both experimentally and theoretically, for over four decades and have numerous applications ranging from textile colorants to high-tech opto-electronic devices.¹⁻⁴ Pioneering work by Marder⁵, Blanchard-Desce⁶, Meerholz⁷, and Würthner et al.⁸

paved the way for their application in nonlinear optics^{3,9}, photorefractivity^{4,7,10}, and solar cells (OSC)¹¹. The donor and acceptor groups present in MCs are linked by ethylene or polyethylene bridges. As a result, a crucial structural characteristic of MCs is the so-called bond-length alternation (BLA) defined as a measure of the difference between single and double carbon-carbon bonds of the polyethylene bridge. Small (large) BLAs indicate increased (decreased) electron delocalization and strong (weak) donor-acceptor coupling, resulting in a red (blue) shift in the spectra.¹² The BLA parameter measures the electron delocalization within a molecule, with smaller BLA values generally indicating lower excitation energies. Conversely, larger BLA values signify reduced delocalization and higher excitation energies, resulting in absorption at higher energy levels. A small or vanishing BLA denotes an electronic structure that is close to the cyanine form, whereas a large positive or negative BLA denotes an increase in the weight of the neutral or the zwitterionic form.¹³ From the theoretical point of view, MC BLA is not accurately described using standard DFT based on the generalized gradient approximation.^{14–16} In this work, we report the importance of optimizing the molecular structure of MCs with double-hybrid density functionals in a polar environment to accurately capture the measured BLA pattern of merocyanines.

The quantitative prediction and comprehension of low-lying excitations in MC molecules are both fundamentally interesting and technologically important. For instance, the calculation of excitation energies provides valuable insights into the photophysical properties of merocyanines^{11,17,18}, including absorption spectra^{12,19}, fluorescence emission²⁰, and photochemical behavior^{16,21}. A standard approach to calculate molecular excitation spectra is time-dependent density-functional theory (TD-DFT) based on various density-functional approximations (DFA). In previous studies it was found that the first excitation energy is overestimated by about 0.3 eV with TD-DFT, even with fourth-rung DFA such as CAM-B3LYP⁶. Here, we assess the performance of TD-DFT based on DFAs up to the fifth rung to reproduce the experimental first singlet excitation energies of a selection of MCs with different donor/acceptor functional groups, denoted as **D1A1**, **D1A2**, **D1A3**, **D2A4**

(see Figure 1). Solvent effects were taken into account using the conductor-like screening polarizable continuum model (CPCM)²². We compared the TD-DFT results with higher-level methods such as the Green function-based Bethe-Salpeter Equation (GW-BSE)²³, the complete active space self-consistent field (CASSCF)²⁴ and the similarity transformed equation of motion coupled cluster theory (STEOM-DLPNO-CCSD)²⁵. Additionally, the time-dependent coupled-perturbed DFT (TDCP-DFT) method²⁶ was applied. This method has been demonstrated to provide highly accurate excitation energies for inorganic solids^{27–29}, and in this work it is applied to molecular systems for the first time. We analyze the electrostatic interaction between merocyanine molecules in the crystalline state by aligning the transition dipole vectors. This method yields deeper insights into the aggregation behavior that influences the optical absorption properties of the merocyanines. Additionally, we analyze distances between the barycenters of adjacent molecules to infer intermolecular coupling, providing a new perspective on the molecular interactions within these systems.

Methods

All molecular structure optimizations and TD-DFT calculations were performed with ORCA version 5.0³⁰. The geometry of the MC molecules was optimized with the DFAs mentioned below, def2-TZVP basis sets³¹ and Grimme’s D3 dispersion correction³². An initial conformer search was performed with CREST³³ combined with the semiempirical GFN1-xTB method³⁴. The most stable conformers were then optimized in gas-phase and in solution applying the CPCM²² solvation model in ORCA.³⁰ All TDDFT calculations are performed with non-equilibrium and linear response PCM regime. The solvent shift of the first excitation energy $\delta S = S_1^{gas} - S_1^{sol}$ is calculated at TD-DFT level and applied to the higher-level methods where the CPCM cannot be applied.

We employed the following density functional approximations (DFA): PBE³⁵, PBE0³⁶, B3LYP^{37–40}, CAM-B3LYP⁴¹, wB97X⁴², B2PLYP⁴³, and basis sets def2-TZVP, def2-TZVPP and def2-QVZPP⁴⁴ for the TD-DFT calculations. In order to investigate the influence of elec-

tron correlation, STEOM-DLPNO-CCSD²⁵ calculations were performed on DFT-optimized geometries using ORCA version 4.2.0.⁴⁵ We utilized two different basis sets (namely def2-SVP and def2-TZVP), and considered up to five singlet states in our calculations, employing standard threshold parameters, including DTol, STol, OThresh, and VThresh, as specified in the ORCA manual. GW-BSE calculations of the optimized MC structures were performed with the MOLGW code⁴⁶ applying the G_nW_0 approximation based on B3LYP^{37,38} wavefunctions obtained with Dunning correlation-consistent polarized triple-zeta (cc-pVTZ) basis sets⁴⁷. We observed that quasiparticle energies converged within a few meV within six iterations. The GW approach takes into account electron correlation and polarization effects around holes and electrons, and provides physically meaningful one-electron energy levels. By solving the Bethe-Salpeter equations (BSE) electron-hole interaction is included for excited states. This approach has been proven to provide reliable results for excitation energies of organic molecules.⁴⁸

TDCP-DFT^{49,50}, also based on B3LYP wavefunctions, was applied as implemented in a locally modified version of CRYSTAL14^{26,51,52}. We used optimized BSSE-corrected triple-zeta plus polarization basis sets (pob-TZVP-rev2).⁵³ The poles of the dynamical polarizability tensor are calculated to approximate the optical transition energies. The TDCP-DFT method only provides dipole allowed transitions and does not account for quadrupole or dipole magnetic effects. In addition, because we used a purely adiabatic approximation for the non-local hybrid kernel, this approach can only determine the fundamental mode of the exciton series. Further, we calculated the dielectric constant of the molecular crystals using the CPHF method in CRYSTAL.^{54,55}

Fractional occupation number weighted electron density (FOD) calculations were conducted using ORCA to assess the partial occupation of frontier orbitals and determine the FOD number (N_FOD).⁵⁶ The FOD number serves as a molecular parameter indicating the presence of "hot" electrons, specifically correlated electrons within the system. Default Density Functional Approximations (DFA) as implemented in ORCA version 4.2.0 were employed

for these FOD calculations.

Furthermore, FOD calculations were utilized as an initial screening tool to determine the active space for further Complete Active Space Self-Consistent Field (CASSCF) calculations.⁵⁷ For the MCs under investigation, various active spaces were considered, spanning from (4,4) to (12,12). Unless otherwise stated, the chosen active space is (12,12). To refine the energy determination of singlet excited states, second-order N-electron valence perturbation theory (NEVPT2) corrections with fully internally contracted (FIC) wavefunctions were incorporated using the CASSCF/NEVPT2-FIC method, which is available in ORCA version 4.2.0.⁴⁵

Unless stated otherwise, the B2PLYP optimized geometries were used for all calculations to achieve consistency. Only the first singlet excited state S_1 was considered for each chromophore, as the higher excited states are outside the visible region of the absorption spectrum (TDDFT artifact), which were not the focus of this work. We compare the computed excited state S_1 of the investigated MCs to experimental absorption maxima obtained from the UV-Vis adsorption measurements.^{2,58-60}

Results and Discussion

The structures of the donor (D) and acceptor (A) units investigated in this study are shown in Figure 1. The four reference systems studied here are classified according to the D/A combinations that define the π -conjugated backbone: **D1A1**, **D1A2**, **D1A3**, and **D2A4** (See Figure 2). The following donor and acceptor groups were selected as representatives of a wide range of MCs, and since experimental data are available for structure and excitation energies: **D1**=5-ethenyl N,N-disubstituted thiophenamine, **D2**=(2Z)-butyl-ethylidene 2,3-dihydro-1,3-benzothiazole ('Fischer base'), **A1**=2-[(5Z)-4-tert-butyl-5-ethylidene-1,3-thiazol-2-ylidene]propanedinitrile, **A2**=(3Z)-5-benzyl-3-ethylidene-2-methyl-4,6-dioxocyclohex-1-ene-1-carbonitrile, **A3**=2-[(2Z)-2-ethylidene-3-oxo-2,3-dihydro-1H-inden-1-yl]propanedinitrile, **A4**=2-

(2-tert-butyl-6-methyl-4H-pyran-4-ylidene)propanedinitrile.

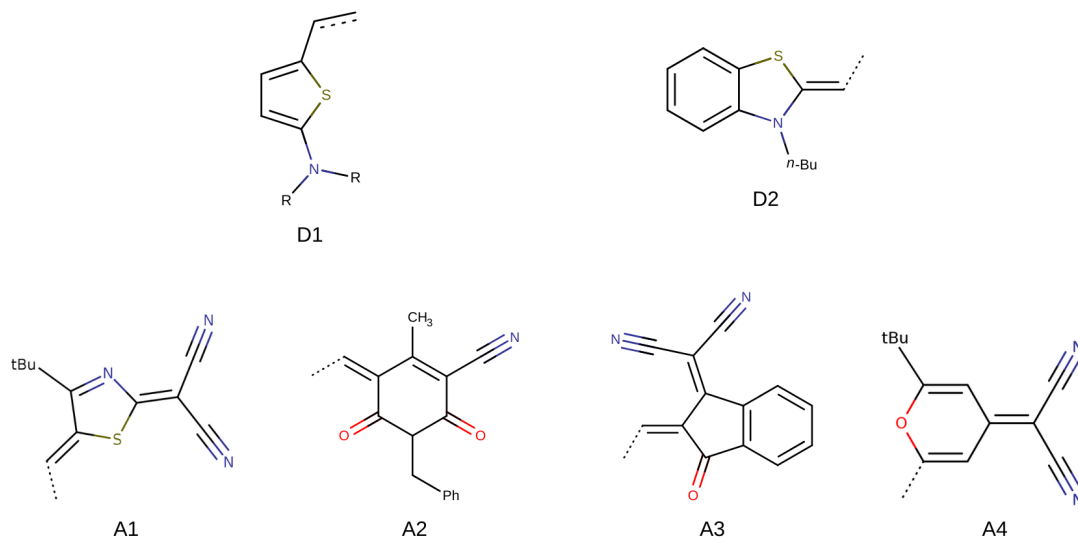


Figure 1: Molecular structures of the donor (D) and acceptor (A) units constituting the merocyanines investigated. R can be either n-butyl(n-bu) or ethyl(Et) group.

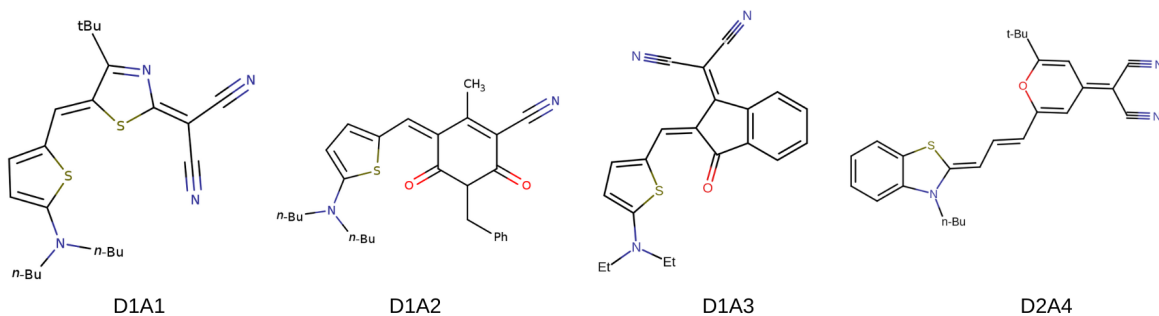


Figure 2: Molecular structures of the investigated merocyanines.

First we discuss the influence of the DFA and the solvent effect on the structures of **D1A1** and **D1A2** with an emphasis on the bond length alternation (BLA).

Geometry optimizations

The accurate description of the ground-state geometry of MCs is challenging for standard DFAs⁶¹. This is due to the presence of two resonance structures, representing a neutral and a zwitterionic form, which require a careful description of static and dynamic correlation effects. Since geometry optimization with more sophisticated methods is cumbersome for screening purposes, standard DFAs have been nonetheless applied to calculate MC geometries. The BLA, as a simple measure of the relative weights of the neutral and zwitterionic forms¹³, has been used to assess the reliability of the theoretical approaches. d_{BLA} is defined as the difference between the average of single and double bond lengths R ($d_{BLA} = \sum_i^N (R_{\text{single}}^i)/N - \sum_j^M (R_{\text{double}}^j)/M$) where N and M are the numbers of single and double bonds, respectively. In general, the bonds connecting the donor and acceptor units are used for BLA calculation, however, we consider the alternating single and double bonds across the π -conjugated backbone of the molecules as suggested by Gildemeister et al.⁶¹ (see also Figure S1 in the Supporting Information). For the sample chromophores of our selection, we compared the BLA as calculated with various DFAs in the gas phase with experimental data obtained from X-ray diffraction (XRD)^{58–61}.

Table 1: Mean absolute deviation (MAD) with respect to experimental structures of d_{BLA} (Å) calculated in the gas phase with various DFAs including PBE, ω B97X, CAM-B3LYP, B3LYP, and B2PLYP with respect to experimental XRD data. All calculations were performed with Grimme’s D3 dispersion correction and def2-TZVP basis set.

Merocyanine	PBE0	ω B97X	CAM-B3LYP	B3LYP	B2PLYP	XRD
D1A1	−0.024	−0.049	−0.039	−0.024	−0.024	−0.001 ^a
D1A2	−0.007	−0.024	−0.017	−0.008	−0.008	0.016 ^b
D1A3	−0.012	−0.026	−0.019	−0.027	−0.012	0.011 ^c
D2A4	0.047	0.071	0.062	0.048	0.048	0.047 ^d
MAD	0.018	0.037	0.029	0.022	0.018	

^a:Reference²; ^b:Reference⁵⁸; ^c:Reference⁵⁹; ^d:Reference⁶⁰;

Among the considered DFAs, the dispersion-corrected double-hybrid functional B2PLYP-D3 and PBE0-D3 provide best agreement with the experiment, also the global hybrid functional B3LYP-D3 combined with def2-TZVP basis sets provide results reasonably closer to the aforementioned functionals. Nonetheless, both double hybrid and global hybrid functionals significantly underestimate the experimental BLA and provide the wrong sign for **D1A2** and **D1A3**, underpinning electronic correlation effects of these MC ground states.

Since UV-Vis absorption spectra are measured in solution, we focus on the effects of solvation on the MC structure in the next section. Previously it was shown that these effects can be effectively addressed using a polarizable continuum method (PCM), by considering highly polar solvents, such as acetone and DMSO¹⁸, or by using a constrained-DFT approach (CDFT)⁶¹. For this purpose, we re-optimized the structures by applying the CPCM with the solvent acetone (in order to show the solvent effect of a polar solvent) and the respective solvents as used in the UV-Vis experiments, dichloromethane (DCM) for D1A1 and D1A3, 1,4-dioxane for D1A2, and dimethylsulfoxide (DMSO) for D2A4. The results are shown in Table 2 and Figure 3.

Table 2: Mean absolute deviation (MAD) of $d_{BLA}(\text{\AA})$ calculated with B2PLYP-D3 and B3LYP-D3 for the MC geometries as optimized in respective solvents.

Merocyanine	Solvent	B2PLYP-D3	B3LYP-D3
D1A1	Acetone	0.013	0.014
	DCM	0.008	0.009
D1A2	Acetone	0.019	0.023
	1,4-dioxane	0.002	0.003
D1A3	Acetone	0.010	0.013
	DCM	0.008	0.010
D2A4	Acetone	0.025	0.022
	DMSO	0.023	0.021
MAD	Acetone	0.010	0.012

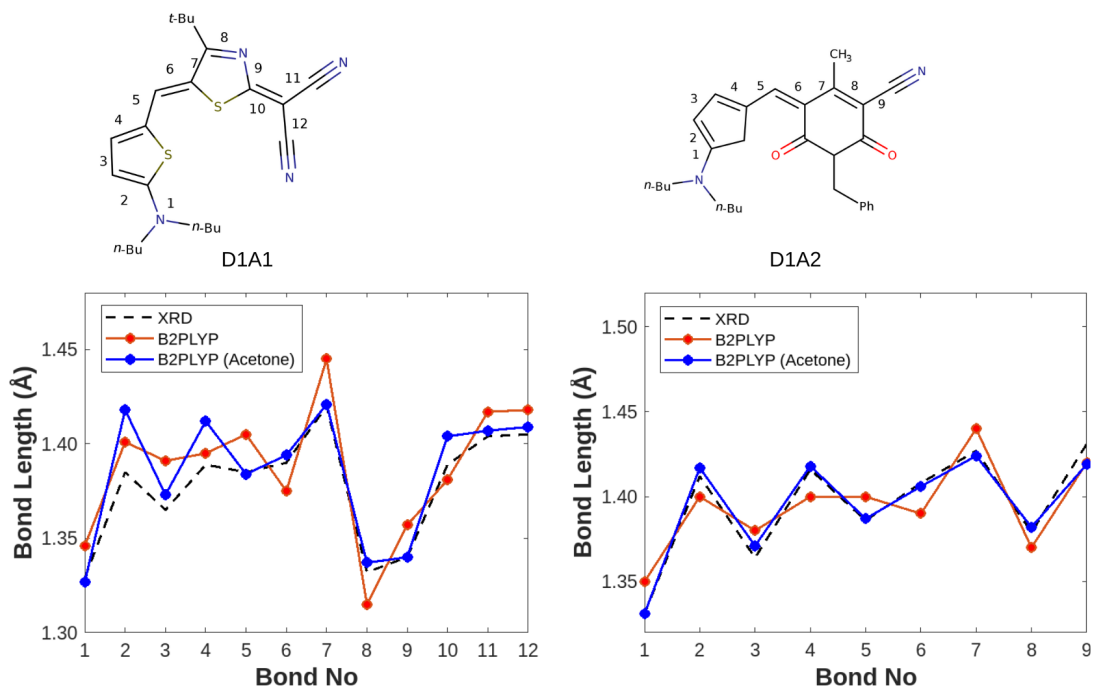


Figure 3: Comparison of calculated and measured bond length alternations of **D1A1** and **D1A2**; black dotted lines: XRD², red solid lines: B2PLYP (gas phase) and blue solid lines: B2PLYP/CPCM (acetone).

Solvent effects on Merocyanine Geometry

The solvatochromic shifts of merocyanine (MC) molecules have been extensively investigated, and we here report that the shifts are dependent on the geometry, namely the bond length alternation (BLA) of the molecule. The solvent polarity changes the equilibrium between the neutral and zwitterionic states, shifting the structure towards one of the two forms.

In a previous study, CDFT has been used to distinguish between the two electronic situations.⁶¹ Here we show that the effects of solvent polarity on the geometry of MCs are crucial. Solvent effects steer the molecule's behavior towards one of two extreme states of cyanine compounds: neutral or zwitterionic. When optimizing the geometry of a merocyanine molecule in a polar solvent like acetone, the Bond Length Alternation (BLA) parameter's sign changes. This shift reflects a transformation in the molecule's arrangement from a zwitterionic state ($d_{BLA} < 0$, indicating electron concentration at one end) to neutral form ($d_{BLA} > 0$, suggesting a more evenly distributed electron pattern) for MC's D1A1,

D1A2 and D1A3. For the structures optimized in acetone, the MAD of the calculated BLA is significantly reduced (from 0.018 to 0.010 for B2PLYP and 0.022 to 0.012 for B3LYP, Table 2). MAD refers to the average of the absolute deviations of the bond length alternation (d_{BLA}) calculated using various density functionals from the experimental XRD data. This indicates that the solvent approximates the electrostatic intermolecular interactions in the bulk which affects the molecular structure. Agreement with the experimental structures is slightly better with B2PLYP-D3 than with B3LYP-D3. Therefore, all subsequent electronic and optical properties calculations were performed on the B2PLYP-D3 optimized structures.

The solvent effects on the excitation energy of MC **D2A4** have been reported experimentally.⁶⁰ Therefore, we calculated the geometry dependence of **D2A4** on the polarity of the solvent (Figure S3). In agreement with previous theoretical studies^{6,60,61} there is a strong dependence of the calculated BLA on the dielectric constant of the solvent. For comparison, we also computed the first excitation energy of molecular crystals of D2A4. The calculation of the dielectric constant of the merocyanine crystals involves computing the components of the dielectric tensor ϵ_{tu} , which can be obtained from the polarizability tensor α_{tu} components as per the equation:

$$\epsilon_{tu} = \delta_{tu} + \frac{\alpha_{tu}}{\epsilon_0 V}$$

where δ_{tu} is Kronecker’s delta, ϵ_0 is the permittivity of vacuum ($1/4\pi$ in the Gaussian system of units), and V is the unit cell volume. The term $\alpha_{tu}/\epsilon_0 V$ represents the first dielectric susceptibility $\chi_{tu}^{(1)}$, which is proportional to the linear coefficient of the derivative of the induced polarization vector $P_t(\mathcal{E})$, as given by the equation:

$$P_t(\mathcal{E}) = \frac{1}{V} [\mu_t(\mathcal{E}) - \mu_t(0)]$$

The dielectric constant is then obtained from the dielectric tensor by taking its trace and computing it in the limit as the frequency (ω) approaches zero, as per the Time-Dependent

Coupled Perturbed (TD-CP) equations. This approach is implemented in the CRYSTAL software, which we used to compute the dielectric constant of the merocyanine crystals.^{51,62} The best agreement between theoretical and experimental structure is obtained when the dielectric constant of the solvent is close to that of the merocyanine crystal. We calculated the dielectric constant of the merocyanine crystals using TDCP-B3LYP method and pob-TZVP-rev2 basis-set. This finding highlights the importance of taking into account solvent effects not only in the calculation of the excited-state wavefunction, but also on the MC geometry when studying the optoelectronic properties.

Method dependence of optoelectronic properties of D1A1

In the following, we assess the accuracy of various DFAs (PBE, PBE0, B3LYP, CAM-B3LYP, and B2PLYP) for the calculation of electronic and optical properties of the MC **D1A1**. The highest occupied molecular orbital (HOMO) energy and the first singlet excitation energy S_1 were considered. While the HOMO energy can be accurately measured experimentally and is directly related to the ionization potential, the experimental determination of the LUMO energy is more challenging and often involves approximations.^{63,64} Therefore, we focused our analysis on the HOMO energy to provide a more reliable assessment of the accuracy of the calculated electronic and optical properties.

Table 3: Optoelectronic properties of D1A1: HOMO energy and singlet $S_0 - S_1$ vertical energy transition in the gas phase in eV. All DFT calculations were performed using the def2/TZVP basis set, G_6W_0 calculations were performed on B3LYP wavefunctions obtained with cc-pVTZ basis sets. All TDDFT calculations were performed on the geometries optimized with the same DFT functionals in gas or solvent (DCM) phase respectively and B3LYP geometry was used for G_6W_0 calculations.

Method	PBE	PBE0	B3LYP	CAM-B3LYP	B2PLYP	G_6W_0	Exp
HOMO (eV)	-4.88	-5.65	-5.40	-6.64	-6.05	-6.59	-5.52 ^a
$S_0 - S_1$ (gas phase)	2.75	2.87	2.84	2.92	2.46	2.05	—

^a:Reference²

The rung four global hybrid functionals PBE0 and B3LYP give a good account of the measured HOMO energy with deviations of ~ 0.1 eV (Table 3). As expected, PBE provides a too-high value due to the self-interaction error, while CAM-B3LYP strongly underestimates the experimental reference value. We performed G_nW_n calculations at different levels including G_0W_0 , G_6W_0 and G_6W_6 , cc-pVDZ and cc-pVTZ basis sets, and found that the present results are converged in terms of GW self-consistency, but not with the basis set size (Table S2 in SI). Due to the limitations of our computer resources, it was not possible to employ cc-pVQZ basis sets. Surprisingly, the G_6W_0 HOMO energies, which should be the best representation of ionization potentials, are more than 1 eV too low. At the moment we have no explanation for this discrepancy.

All TD-DFT methods strongly overestimate the vertical excitation energy, by 0.7-0.9 eV with respect to the experimental λ_{max} energy. We verified by a systematic increase of the basis set size from def2-TZVP to def2-TZVPP and def2-QVZPP (see Table S1 in the Supporting Information), that this is not a basis set incompleteness error. Such an overestimation has been observed previously for similar systems.^{65,66} As we compare the computed vertical excitation energy S_1 of the investigated MCs to experimental absorption maxima, it can lead to an overestimation of computed energies. In order to simulate the band shape and the origin of the spectra accurately nuclear effects (e.g., vibronic effects and Wigner ground state sampling) can be included.^{67,68} It is important to note that the neglect of vibronic effects in our calculations can lead to a systematic error, i.e. ~ 0.1 eV in the predicted excitation energies as suggested by Fang et al.⁶⁹ and Santoro et al.⁶⁷ MCs have been shown to exhibit large solvatochromic effects, with both hypsochromic and bathochromic shifts measured.⁶⁰ The effect of structural changes due to solvent effects will be discussed later. First, we consider the possibility that the discrepancies between experiment and theory are due to the conformational flexibility of MCs, which requires sampling of spectra for many configurations. Previous studies by Tirri et al., Georg et al. and Coutinho et al. report improvements in the description of excitation spectra of merocyanines using Monte Carlo

sampling of molecular configurations.^{12,70,71} We tested the conformational sampling tool CREST and performed sampling of MC geometries in gas phase as well as solvent phase using iMTD-sMTD algorithm and GFN1-XTB Hamiltonian. A conformer study of **D1A1** is reported in the next section.

Conformers of **D1A1**

In the neutral ground state, **D1A1** has a planar π -conjugated backbone. However, the *t*-butyl groups are rather flexible and free to rotate. Since the relative orientation of these groups may affect the optical excitation spectrum in terms of band broadening and band shift, we calculated (at TD-DFT level) the excitation energy of 356 most stable conformers of **D1A1** obtained by CREST³³ (Figure 4). However, the broadening effect due to conformation sampling is quite small (~ 0.04 eV in gas phase and 0.10 eV in DCM solution). The TD-DFT S_1 excitation energy ranges from 2.68 to 2.72 eV in the gas phase and from 2.59 to 2.69 eV in the solvent (CPCM/DCM). These values suggest a systematic error of ~ 0.1 eV in the computed excitation energies using TDDFT methods. However, these excitation energies are well above 1.90 eV (λ_{max}) obtained from UV-Vis experiment.²

In the present study, we performed a comprehensive analysis by investigating both the monomeric and dimeric forms of merocyanines and comparing them with the available experimental spectra. This approach is crucial because it helps to understand the aggregation behavior of merocyanines in solution. We also explored the possibility of red-shift in the excitation energy going from the MC monomers to the dimers, all due to mutual polarization as suggested by Tirri et al.¹² We used the iMTD-sMTD method as implemented in CREST to perform conformational sampling on two **D1A1** molecules positioned side-by-side. In the gas phase, the **D1A1** molecules form stacked antiparallel dimers, whereas in dichloromethane they are oriented orthogonal to each other (Figure 4). This shows the significant influence of the solvent on the structural characteristics of MCs. The excitation energies of the 197 lowest-energy dimer configurations in gas phase and dichloromethane solvent are shown in

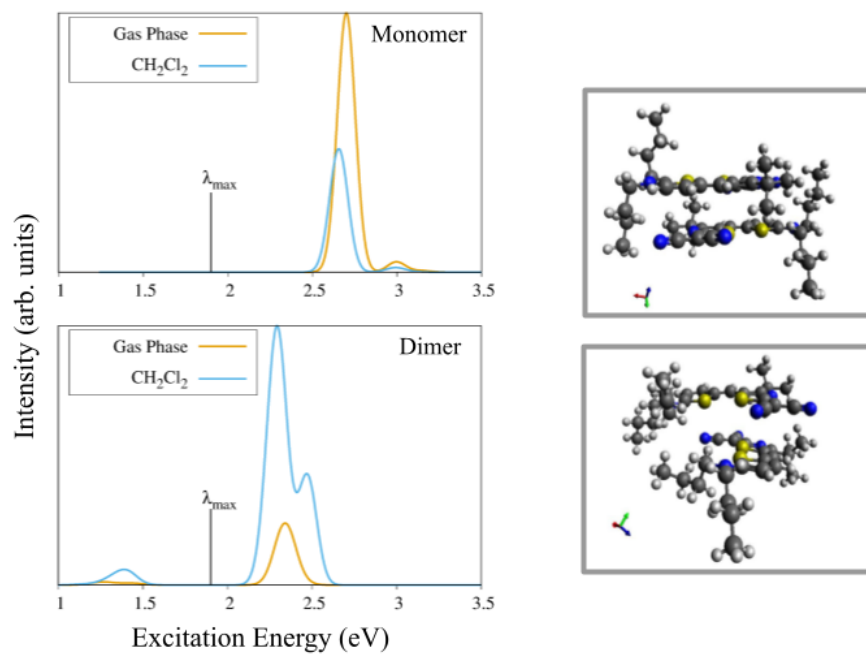


Figure 4: Boltzmann weighted absorption spectra of 356 most stable **D1A1** monomer conformations (top left) and 197 most stable dimer configurations (bottom left) as obtained via CREST, calculated using TD-DFT at B3LYP/def2-TZVP level. The experimental λ_{max} value is shown by the black vertical line at 1.9 eV.² The most stable conformers of D1A1 dimers in gas phase (top right) and DCM solvent (bottom right) are reported.

Figure 4. In the dimer configuration, S_1 energy varies based on the specific geometry and electronic structure of the dimers. This is evident from the transitions observed around 1.5 eV, indicating that S_1 can be active or dark depending on the dimer’s geometry. In the case of the antiparallel configuration (H-like dimer stacking), the higher energy states (S_2 and S_3) gain oscillator strength, while S_1 becomes dark or weakly allowed. In monomer spectra, the weak peaks observed at 2.9-3.0 eV represent transitions to a higher excited state (S_2) of the molecule (see Figure 4).

Excitation energies in gas-phase and in solution

We examined different levels of theory, including TD-DFT, GW-BSE, STEOM-DLPNO-CCSD, CASSCF, and TDCP-DFT, in search of an efficient and accurate computational approach for characterizing the first excitation energy of MCs. It has been shown before, that TD-DFT significantly overestimates the excitation energies of merocyanines^{6,19}, which was attributed to the lack of differential correlation energy in DFT. Double-hybrid functionals (e.g. B2PLYP) do not fully alleviate this problem, although they improve the description of excited states in general.^{43,72} The treatment of electron correlation effects using coupled cluster (CC) theory,⁷³ or the Bethe-Salpeter approach based on Green function with screened Coulomb interaction (GW-BSE)^{50,74,75} approaches provided accurate excitation energies, however at high computational cost.

In the case of the MC’s examined in this study, N_FOD values ranged from 0.5 to 0.7, indicative of a single-reference character for describing the electronic structure of the ground state. We further used the N_FOD analysis for active space determination in CASSCF/NEVPT2-FIC calculations. Active spaces (12,12) are used for MC D1A1 and D1A3 and (4,4) for D1A2.

TD-DFT is computationally efficient and allows to take solvent effects into account via continuum models such as CPCM. This is presently not possible with the more sophisticated methods. We distinguished between two kinds of solvent effects: (I) excitation energy shifts

for a given structure, and (II) structural changes. Both solvent shifts (δS) were calculated with B2PLYP/def2-TZVP at TDDFT level (Table 5) and added to the GW-BSE, STEOM-DLPNO-CCSD, CASSCF/NEVPT2, and TDCP-DFT gas-phase results (Table 4) in Table 6.

In the first series of calculations, we used the same geometries of the MCs in gas-phase and solvent (effect I). Table 4 shows the gas-phase results, in Table 6 the S_1 energies obtained for the B2PLYP gas-phase structures are shifted by δS calculated with TD-B2PLYP.

Table 4: S_0 - S_1 energy (eV) for selected MCs calculated using TD-DFT (B2PLYP-D3), GW-BSE (B3LYP), STEOM-DLPNO-CCSD, CASSCF/NEVPT2, TDCP-DFT. MAD (eV) for individual methods compared to the experimental excitation energy (B2PLYP geometry and excitation energy calculations performed in gas phase.)

Merocyanine	TD-DFT	GW-BSE	STEOM-DLPNO-CCSD	CASSCF/NEVPT2-FIC	TDCP-DFT	Exp.
D1A1	2.46	2.06	1.87	2.03	1.90	1.90 ^a
D1A2	2.93	2.62	2.47	2.26	2.37	2.31 ^b
D1A3	2.59	2.37	2.01	2.38	2.31	2.15 ^c
D2A4	2.82	2.70	—	—	2.48	2.15 ^d
MAD	0.57	0.34	0.11	0.14	0.14	

^a: Reference², ^b: Reference⁵⁸, ^c: Reference⁵⁹, ^d: Reference⁶⁰

Table 5: S_0 - S_1 energies and solvent shift $\delta S = E_{ex}^{gas} - E_{ex}^{sol}$ (eV) for the selected MCs calculated using B2PLYP/def2-TZVP and CPCM in ORCA. Fixed gas-phase geometries obtained with B2PLYP/def2-TZVP are used.

Merocyanine	Solvent	gas phase	solution	δS
D1A1	DCM	2.46	2.19	-0.27
D1A2	1,4-dioxane	2.93	2.66	-0.27
D1A3	DCM	2.59	2.27	-0.32
D2A4	DMSO	2.82	2.37	-0.45

Table 6: S_0 - S_1 energies (eV) after addition of the TD-DFT solvent shift δS for the same MCs and methods as in Table 4; MAD for individual methods with respect to the experimental excitation energy..

Merocyanine	TD-DFT	GW-BSE	STEOM-DLPNO-CCSD	CASSCF/NEVPT2-FIC	TDCP-DFT	Exp.
D1A1	2.19	1.79	1.60	1.76	1.63	1.90
D1A2	2.66	2.35	2.00	1.99	2.10	2.31
D1A3	2.27	2.05	1.69	2.06	1.99	2.15
D2A4	2.37	2.25	—	—	2.03	2.15
MAD	0.25	0.09	0.36	0.18	0.19	

By adding the solvent shifts, GW-BSE S_1 results are considerably improved, the MAD decreases from 0.34 eV to 0.09 eV. A similar trend is observed for TD-B2PLYP, however, the MAD is still much larger, 0.25 eV. STEOM-DLPNO-CCSD and CASSCF/NEVPT2 (MAD=0.36 and 0.18 eV) reproduce the experimental S_1 energies more accurately without solvent shift (MAD=0.11 and 0.14 eV, respectively). We noted that the STEOM-DLPNO-CCSD and CASSCF/NEVPT2 calculations give comparable results if a polar solvent-optimized geometry is considered for $S_0 - S_1$ computation. The excitation energy so obtained are 1.73 and 2.04 eV respectively for MC D1A1 with the geometry optimized using CPCM/Acetone. For the gas-phase optimized geometry of MCs, experimental S_1 energies are efficiently and closely described with TDCP-DFT. The MAD is not significantly changed after adding the solvent shifts (MAD=0.14 and 0.19 eV, respectively). The higher accuracy of TDCP-DFT S_1 energies compared to TD-DFT can be attributed to the better screening of electrons in the hole for the extended- π delocalization of MCs. In the present case, TDCP-DFT is a more efficient alternative to STEOM-DLPNO-CCSD and CASSCF/NEVPT2. Another advantage is that this method can also be applied to periodic calculations of molecular crystals (see next section), which is at present not possible with CCSD and CASSCF. GW-BSE calculations with VASP⁷⁶⁻⁷⁸ were not successful, neither for the isolated molecules nor for molecular crystals, due to limitations of our computational resources.

In the second step, we optimized the MC structures in the solution with B2PLYP (effect II). Since it is known that the molecular geometries are significantly affected by solvent effects,¹⁸ we optimized the MC structures under conditions that are as close as possible to the experiment. For this purpose, we employed toluene ($\epsilon = 2.4$) for **D1A1**, **D1A2**, **D1A3** and chloroform ($\epsilon = 4.9$) for **D2A4**, respectively. The dielectric constants of these solvents are close to those of the molecular crystals, obtained with TDCP-DFT (see Table 9). Indeed we obtained improved BLA compared to other solvents (see Table 2) in this way. BLA indirectly reflects the degree of π -electron delocalization in a conjugated molecular system. Greater electron delocalization results in a more uniform molecular structure, such as equalized bond

lengths, leading to smaller BLA values. A more delocalized electronic structure, however, is connected with a low energy gap between the occupied and unoccupied molecular orbitals (typically the HOMO and LUMO), thus leading to low values of the excitation energies (see Fig 5). In this context, BLA can be associated with the electronic absorption spectrum of individual MC molecules. MCs showing large values of BLA (i.e. alternated structures) result in single-molecule absorption spectra blue-shifted with respect to MCs with vanishing BLA. This confirms the high importance of the solvent effects on MC structure, which in turn affects optoelectronic properties reported in Table 7.

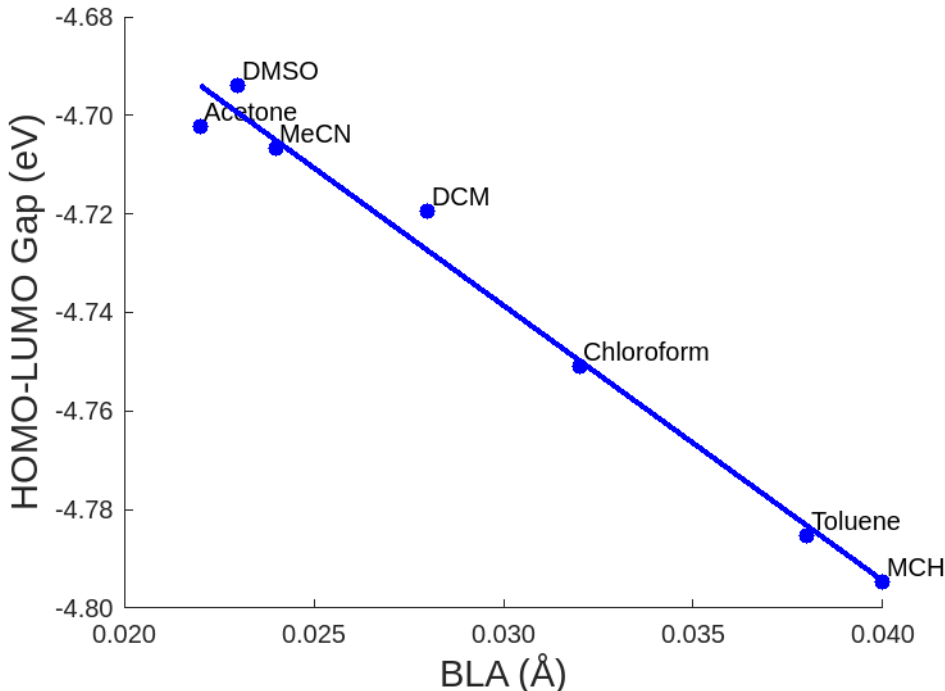


Figure 5: The bond length alternation dependence of MC D2A4 on the HOMO-LUMO gap of the solution calculated at B2PLYP/D3 level with def2-TZVP basis set. Actual values are represented by circles, solid line shows a linear fit of the data points.

For a second series of excited-state calculations, we therefore, used the MC geometries obtained by B2PLYP in the respective solvents of the solution experiments, DCM for **D1A1** and **D1A3**, 1,4-dioxane for **D1A2**, and DMSO for **D2A4**. After taking into account both the geometry change and the solvent shift in solution, Tables 7 and 8, GW-BSE again outperforms all other methods (MAD = 0.05 and 0.07 eV, respectively). Also, TD-DFT

Table 7: S_0 - S_1 energies (eV) obtained for MC structures optimized with the solvents that have similar dielectric constant as the respective molecular crystal. The S_1 energies are shifted by δS of Table 5 and MAD is calculated with respect to the experimental excitation energy.

Merocyanine	Solvent ^a	Solvent ^b	TD-DFT	GW-BSE	TDGP-DFT	Exp.
D1A1	Toluene	DCM	2.16	1.83	1.52	1.90
D1A2	Toluene	1,4-dioxane	2.64	2.32	2.10	2.31
D1A3	Toluene	DCM	2.29	2.05	2.01	2.15
D2A4	Chloroform	DMSO	2.34	2.18	1.99	2.15
MAD			0.23	0.05	0.22	

^a: Solvent used for geometry optimization, ^b: Solvent used in TDDFT for excitation energy calculation.

results are further improved while TDGP-DFT excitation energies are again not affected much.

Table 8: S_0 - S_1 energies (eV) obtained for MC structures optimized with B2PLYP in the respective solvents shifted by δS of Table 5. MAD with respect to the experimental excitation energy.

Merocyanine	Solvent	TD-DFT	GW-BSE	TDGP-DFT	Exp.
D1A1	DCM	2.10	1.75	1.43	1.90
D1A2	1,4-dioxane	2.64	2.32	2.10	2.31
D1A3	DCM	2.30	2.04	1.99	2.15
D2A4	DMSO	2.31	2.15	1.94	2.15
MAD		0.21	0.07	0.26	

Excitation energies in molecular crystals

We applied the TDGP-DFT method to calculate the excitation energy of merocyanines. For the calculation of the MC crystal’s excitation energy and dielectric constant, the positions of hydrogen atoms were optimized starting from the XRD data for the complete unit cell, and the optimized unit cell structure was used for the TDGP-DFT calculations. For the gas phase calculations, the B2PLYP geometry of the molecules was used. The excitation

energy of the MC is 0.1-0.3 eV lower in the molecular crystals than in gas phase except for P1-D1A1. (Table 9). The corresponding crystal structures and crystallographic data are shown in Figure S5 and Table S3. Figure S4 shows the calculated mean dynamical polarizability (MDP) of the two **D1A1** molecular crystals along the three crystallographic directions. The first and only observed absorption peak was detected in all three crystallographic orientations at 1.89 eV. In Table 9 we also report the difference in excitation energy of two D1A1 polymorphs denoted as P1 (CCDC 2073437) and P2 (CCDC 2073438).⁶¹ The excitation energy of P1-D1A1 and P2-D1A1 differ by 0.04 and -0.09 eV, respectively, from the excitation energy of gas phase D1A1 (dashed lines in Figure 6). Since it is known that such shifts are caused by intermolecular coupling of transition dipoles (the so-called J- and H-couplings)^{79,80}, we inserted the transition dipole vectors (calculated for gas-phase D1A1 at PBE/D3/def2-TZVPP level) in the unit cells. This representation of P1-D1A1 and P2-D1A1 suggests weak couplings in the two polymorphs (see Figure S7 in the SI). Consequently, the shifts of the S_1 peaks with respect to isolated molecules are relatively small compared to ordered aggregates on surfaces⁸⁰.

Table 9: Dielectric constants and excitation energies (eV) of the molecular crystals calculated using TDCP-DFT at B3LYP/pob-TZVP level

Merocyanine	Dielectric constant	Excitation energy	
		Crystal	Gas phase
P1-D1A1	2.69	1.93	1.89
P2-D1A1	2.69	1.80	1.89
D1A2	2.66	2.29	2.37
D1A3	3.12	2.04	2.31
D2A4	5.15	2.18	2.48

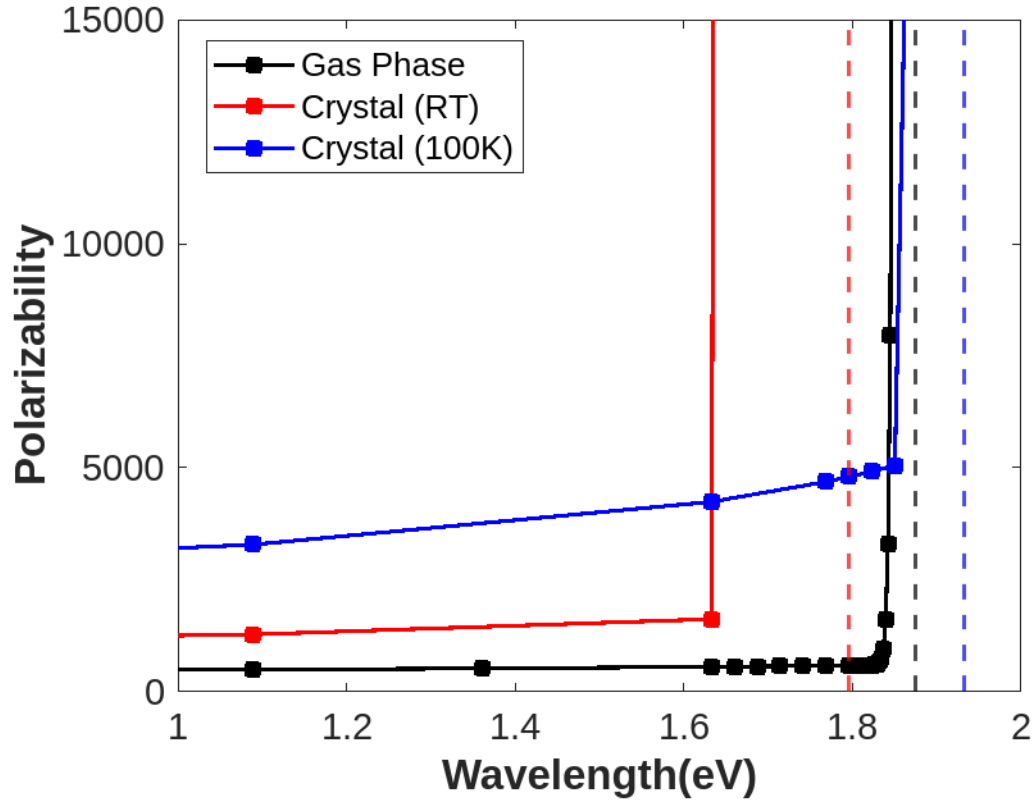


Figure 6: Energy dependence of the many-body polarizability tensor for two **D1A1** polymorphs measured at 100K and room temperature (RT) computed using TDCP-B3LYP. The dynamical polarizabilities are represented by diamonds, solid lines serve as guide to the eye. Red and blue dashed lines represent the optical gap of the crystal structures at the respective temperatures.

Conclusions

We calculated the structural and optoelectronic properties of selected MCs with different donor (D) and acceptor (A) chromophores for which experimental absorption spectra have been reported earlier. Excitation energies were calculated with the TD-DFT, GW-BSE, STEOM-DLPNO-CCSD, CASSCF/NEVPT2, and TDCP-DFT methods. Using the hybrid DFT functionals PBE0 and B3LYP, the experimental ionization energy is best reproduced. Surprisingly, the G_6W_0 method gave too low HOMO energies. However, for the calculation of the first excitation energy, GW-BSE was by far the most accurate approach. The accuracy was further improved by taking into account the geometry changes and solvent shifts in solution. TD-DFT methods overestimate the first excitation energy, which was also observed in previous studies. The more sophisticated STEOM-DLPNO-CCSD and CASSCF/NEVPT2 methods also provide accurate excitation energies but at much higher computational cost. Furthermore, no systematic improvement was possible by adding the solvent shifts obtained with TD-DFT. The TDCP-B3LYP method, which has been previously applied only for crystalline semiconductors and insulating materials, was extended to organic molecules and molecular crystals. In the gas phase, its accuracy is comparable to GW-BSE, STEOM-DLPNO-CCSD, CASSCF/NEVPT2, but it can also not be systematically improved by TD-DFT solvent shifts. We observed a lowering of the first excitation energy in the solids compared to the gas-phase molecule due to exciton coupling. The excitation energy of MCs exhibits sensitivity to the crystal structure. However, in the solid state, the intermolecular coupling of transition dipoles is relatively weak, resulting in modest variations in excitation energy.

Supporting Information

Supporting information includes BLA pathways of MC’s and comparative line graphs illustrating bond length variations of different MCs using diverse functionals; Basis set depen-

dence of $S_0 - S_1$ and HOMO energy for D1A1; BLA vs ϵ graph for D2A4; Polarizability tensors of MC D1A1 along the three crystallographic axis are provided along with crystallographic Parameters and molecular crystal structures of all MCs; Transitional dipole moment vectors of MC's and representative image of the crystal structures using dipole moment vectors.

Acknowledgement

The authors gratefully acknowledge funding from the DFG (RTG-2591 *TIDE Template-designed Organic Electronics*), and the computer resources from the HPC Centre at the University of Bonn. This research was supported in part by the University of Pittsburgh Center for Research Computing through the resources provided. Specifically, this work used the H2P cluster, which is supported by NSF award number OAC-2117681. D.F. gratefully acknowledges N. Gildemeister and S. Lekat for their initial explorative works on the excited states of merocyanines and the computer center "Regionales Rechenzentrum der Universität zu Köln" (RRZK).

References

- (1) Mishra, A.; Behera, R. K.; Behera, P. K.; Mishra, B. K.; Behera, G. B. Cyanines during the 1990s: A Review. *Chem. Rev.* **2000**, *100*, 1973–2011.
- (2) Bürckstümmer, H.; Tulyakova, E. V.; Deppisch, M.; Lenze, M. R.; Kronenberg, N. M.; Gsänger, M.; Stolte, M.; Meerholz, K.; Würthner, F. Efficient solution-processed bulk heterojunction solar cells by antiparallel supramolecular arrangement of dipolar donor-acceptor dyes. *Angewandte Chemie - International Edition* **2011**, *50*, 11628–11632.
- (3) Marder, S. R.; Gorman, C. B.; Meyers, F.; Perry, J. W.; Bourhill, G.; Bredas, J.-L.; Pierce, B. M.; Marder, S. R.; Gorman, C. B.; Perry, J. W. et al. A Unified Description

- of Linear and Nonlinear Polarization in Organic Polymethine Dyes. *Science* **1994**, *265*, 632–635.
- (4) Meerholz, K.; Volodlin, B.; Sandalphon,; Kippelen, B.; Peyghambarian, N. A photorefractive polymer with high optical gain and diffraction efficiency near 100% . *Nature* **1994**, *371*, 497–500.
 - (5) Marder, S. R.; Cheng, L.-T.; Tiemann, B. G.; Friedli, A. C.; Blanchard-Desce, M.; Perry, J. W.; Skindhøj, J. Large First Hyperpolarizabilities in Push-Pull Polyenes by Tuning of the Bond Length Alternation and Aromaticity. *Science* **1994**, *263*, 511–514.
 - (6) Parthasarathy, V.; Pandey, R.; Stolte, M.; Ghosh, S.; Castet, F.; Würthner, F.; Das, P. K.; Blanchard-Desce, M. Combination of Cyanine Behaviour and Giant Hyperpolarisability in Novel Merocyanine Dyes: Beyond the Bond Length Alternation (BLA) Paradigm. *Chem. Eur. J.* **2015**, *21*, 14211–14217.
 - (7) Würthner, F.; Wortmann, R.; Matschiner, R.; Lukaszuk, K.; Meerholz, K.; DeNardin, Y.; Bittner, R.; Brauchle, C.; Sens, R.; Wühner, K. E. et al. Merocyanine Dyes in the Cyanine Limit: A New Class of Chromophores for Photorefractive Materials. *Angew. Chem. Int. Ed.* **1997**, *36*, 2765–2768.
 - (8) Bürckstümmer, H.; Kronenberg, N. M.; Gsänger, M.; Stolte, M.; Meerholz, K.; Würthner, F. Tailored merocyanine dyes for solution-processed BHJ solar cells. *J. Mater. Chem.* **2010**, *20*, 240–243.
 - (9) Gorman, C. B.; Marder, S. R. An investigation of the interrelationships between linear and nonlinear polarizabilities and bond-length alternation in conjugated organic molecules. *Proc. Natl. Acad. Sci. USA* **1993**, *90*, 11297–11301.
 - (10) Würthner, F.; Wortmann, R.; Meerholz, K. Chromophore Design for Photorefractive Organic Materials. *Chem. Phys. Chem.* **2002**, *3*.

- (11) Würthner, F.; Meerholz, K. Systems chemistry approach in organic photovoltaics. *Chem. Eur. J.* **2010**, *16*, 9366–9373.
- (12) Tirri, B.; Mazzone, G.; Ottochian, A.; Gomar, J.; Raucci, U.; Adamo, C.; Ciofini, I. A combined Monte Carlo/DFT approach to simulate UV-vis spectra of molecules and aggregates: Merocyanine dyes as a case study. *J. Comput. Chem.* **2021**, 1054–1063.
- (13) Brückner, C.; Engels, B. Benchmarking Ground-State Geometries and Vertical Excitation Energies of a Selection of P-Type Semiconducting Molecules with Different Polarity. *J. Chem. Phys. A* **2015**, *119*, 12876–12891.
- (14) Ciofini, I.; Adamo, C.; Chermette, H. Effect of self-interaction error in the evaluation of the bond length alternation in trans-polyacetylene using density-functional theory. *J. Chem. Phys.* **2005**, *123*, 224103.
- (15) Jacquemin, D.; Perpète, E. A.; Ciofini, I.; Adamo, C. Assessment of recently developed density functional approaches for the evaluation of the bond length alternation in polyacetylene. *Chem. Phys. Lett.* **2005**, *405*, 376–381.
- (16) Mustroph, H.; Reiner, K.; Senns, B.; Mistol, J.; Ernst, S.; Keil, D.; Hennig, L. The effects of substituents and solvents on the ground-state π -electronic structure and electronic absorption spectra of a series of model merocyanine dyes and their theoretical interpretation. *Chem. Eur. J.* **2012**, *18*, 8140–8149.
- (17) Chen, K. W.; Huang, C. W.; Lin, S. Y.; Liu, Y. H.; Chatterjee, T.; Hung, W. Y.; Liu, S. W.; Wong, K. T. Merocyanines for vacuum-deposited small-molecule organic solar cells. *Org. Electron.* **2015**, *26*, 319–326.
- (18) Brückner, C.; Walter, C.; Stolte, M.; Braïda, B.; Würthner, F.; Engels, B.; Brückner, C.; Walter, C.; Stolte, M.; Braïda, B. et al. Structure – Property Relationships for Exciton and Charge Reorganization Energies of Dipolar Organic Semiconductors : A Combined

- Valence Bond Self-Consistent Field and Time-Dependent Hartree-Fock and DFT Study of Merocyanine Dyes. *J. Phys. Chem. C* **2015**, *119*, 17602–17611.
- (19) Guillaume, M.; Champagne, B. B.; Zutterman, F. Investigation of the UV/Visible Absorption Spectra of Merocyanine Dyes Using Time-Dependent Density Functional Theory. *J. Phys. Chem. A* **2006**, *110*, 13007–13013.
- (20) Kulinich, A. V.; Mikitenko, E. K.; Ishchenko, A. A. Synthesis, electronic structure and spectral fluorescent properties of vinylogous merocyanines derived from 1,3-dialkylbenzimidazole and malononitrile. *Spectrochim. Acta - A: Mol. Biomol. Spectrosc.* **2017**, *171*, 317–324.
- (21) Zhao, G.; Yang, Y.; Zhang, C.; Song, Y.; Li, Y. The theoretical study of excited-state intramolecular proton transfer of N, N,-bis (salicylidene)-(2-(3,4-diaminophenyl) benzothiazole). *J. Lumin.* **2021**, *230*.
- (22) Barone, V.; Cossi, M. Quantum Calculation of Molecular Energies and Energy Gradients in Solution by a Conductor Solvent Model. *J. Phys. Chem. A* **1998**, *102*, 1995–2001.
- (23) Salpeter, E.; Bethe, H. A Relativistic Equation for Bound-State Problems. *Phys. Rev.* **1951**, *84*, 1232–1242.
- (24) Roos, B. O.; Taylor, P. R.; Sigbahn, P. E. A complete active space SCF method (CASSCF) using a density matrix formulated super-CI approach. *Chem. Phys.* **1980**, *48*, 157–173.
- (25) Berraud-Pache, R.; Neese, F.; Bistoni, G.; Robert, R.; Izsak, I. Unveiling the Photo-physical Properties of Boron-dipyrromethene Dyes Using a New Accurate Excited State Coupled Cluster Method. *J. Chem. Theory Comput.* **2019**, *16*, 564–575.

- (26) Bernasconi, L.; Tomić, S.; Ferrero, M.; Rérat, M.; Orlando, R.; Dovesi, R.; Harrison, N. M. First-principles optical response of semiconductors and oxide materials. *Phys. Rev. B* **2011**, *83*.
- (27) Webster, R.; Bernasconi, L.; Harrison, N. M. Optical properties of alkali halide crystals from all-electron hybrid TD-DFT calculations. *J. Chem. Phys.* **2015**, *142*.
- (28) Tomić, S.; Bernasconi, L.; Searle, B. G.; Harrison, N. M. Electronic and optical structure of wurtzite CuInS₂. *J. Phys. Chem. C* **2014**, *118*, 14478–14484.
- (29) Živković, A.; De Leeuw, N. H.; Searle, B. G.; Bernasconi, L. Electronic Excitations in Copper Oxides: Time-Dependent Density Functional Theory Calculations with a Self-Consistent Hybrid Kernel. *J. Phys. Chem. C* **2020**, *124*, 24995–25003.
- (30) Neese, F. Software update: The ORCA program system—Version 5.0. *Wiley Interdiscip. Rev. Comput. Mol. Sci.* **2022**, *12*.
- (31) Weigend, F.; Ahlrichs, R. Balanced basis sets of split valence, triple zeta valence and quadruple zeta valence quality for H to Rn: Design and assessment of accuracy. *Phys. Chem. Chem. Phys.* **2005**, *7*, 3297–3305.
- (32) Grimme, S.; Ehrlich, S.; Goerigk, L. Effect of the damping function in dispersion corrected density functional theory. *J. Comput. Chem.* **2011**, *32*, 1456–1465.
- (33) Grimme, S.; Li, R.; Pccp, . P.; Pracht, P.; Bohle, F. Automated exploration of the low-energy chemical space with fast quantum chemical methods. *Phys. Chem. Chem. Phys* **2020**, *22*, 7169.
- (34) Grimme, S.; Bannwarth, C.; Shushkov, P. A Robust and Accurate Tight-Binding Quantum Chemical Method for Structures, Vibrational Frequencies, and Noncovalent Interactions of Large Molecular Systems Parametrized for All spd-Block Elements (Z = 1-86). *J. Chem. Theory Comput.* **2017**, *13*, 1989–2009.

- (35) Perdew, J. P.; Burke, K.; Ernzerhof, M. Generalized Gradient Approximation Made Simple. *Phys. Rev. Lett.* **1996**, *77*, 3865–3868.
- (36) Adamo, C.; Barone, V. Toward reliable density functional methods without adjustable parameters: The PBE0 model. *J. Chem. Phys.* **1999**, *110*, 4775.
- (37) Becke, A. D. Density-functional thermochemistry. III. The role of exact exchange. *J. Chem. Phys.* **1993**, *98*, 5648.
- (38) Lee, C.; eitao Yang,; Parr, R. G. Development of the Colic-Salvetti correlation-energy formula into a functional of the electron density. *Phys. Rev. B* **1988**, *37*, 785–789.
- (39) Vosko, S. H.; Wilk, L.; Nusair, M. Accurate spin-dependent electron liquid correlation energies for local spin density calculations: a critical analysis1. *J. Phys.* **1980**, *58*, 1200.
- (40) Stephens, P. J.; Devlin, F. J.; Chabalowski, C. F.; Frisch, M. J. Ab Initio Calculation of Vibrational Absorption and Circular Dichroism Spectra Using Density Functional Force Fields. *J. Phys. Chem.* **1994**, *98*.
- (41) Yanai, T.; Tew, D. P.; Handy, N. C. A new hybrid exchange-correlation functional using the Coulomb-attenuating method (CAM-B3LYP). *Chem. Phys. Lett.* **2004**, *393*, 51–57.
- (42) Chai, J.-D.; Head-Gordon, M. Systematic optimization of long-range corrected hybrid density functionals. *J. Chem. Phys.* **2008**, *128*, 084106.
- (43) Grimme, S.; Neese, F. Double-hybrid density functional theory for excited electronic states of molecules. *J. Chem. Phys.* **2007**, *127*, 224108.
- (44) Weigend, F.; Ahlrichs, R. Balanced basis sets of split valence, triple zeta valence and quadruple zeta valence quality for H to Rn: Design and assessment of accuracy. *Phys. Chem. Chem. Phys.* **2005**, *7*, 3297–3305.
- (45) Neese, F. Software update: the ORCA program system, version 4.0. *Wiley Interdiscip. Rev. Comput. Mol. Sci.* **2018**, *8*, e1327.

- (46) Bruneval, F.; Rangel, T.; Samia M., H.; Shao, M.; Yang, C.; Neaton, J. B. Molgw 1: Many-body perturbation theory software for atoms, molecules, and clusters. *Computer Phys. Commun.* **2016**, *208*, 149–161.
- (47) Dunning, T. H. Gaussian basis sets for use in correlated molecular calculations. I. The atoms boron through neon and hydrogen. *J. Chem. Phys* **1989**, *90*, 1007.
- (48) Bruneval, F.; Hamed, S. M.; Neaton, J. B. A systematic benchmark of the ab initio Bethe-Salpeter equation approach for low-lying optical excitations of small organic molecules. *J. Chem. Phys.* **2015**, *142*, 244101.
- (49) Runge, E.; Gross, E. K. U. Density-Functional Theory for Time-Dependent Systems. *Physical Review Letters* **1984**, *52*, 997–1000.
- (50) Onida, G.; Reining, L.; Rubio, A. Electronic excitations: density-functional versus many-body Green’s-function approaches. *Rev. Mod. Phys.* **2002**, *74*, 601–659.
- (51) Dovesi, R.; Orlando, R.; Erba, A.; Zicovich-Wilson, C. M.; Civalleri, B.; Casassa, S.; Maschio, L.; Ferrabone, M.; De La Pierre, M.; D’Arco, P. et al. CRYSTAL14: A program for the ab initio investigation of crystalline solids. *Int. J. Quant. Chem.* **2014**, *114*, 1287–1317.
- (52) Bernasconi, L.; Webster, R.; Tomic, S.; Harrison, N. M. Optical response of extended systems from time-dependent Hartree-Fock and time-dependent density-functional theory. *J. Phys. Conf. Ser.* **2012**, *367*, 012001.
- (53) Laun, J.; Bredow, T. BSSE-corrected consistent Gaussian basis sets of triple-zeta valence with polarization quality of the fifth period for solid-state calculations. *J. Comput. Chem.* **2022**, *43*, 839–846.
- (54) Kirtman, B.; Gu, F. L.; Bishop, D. M. Extension of the Genkin and Mednis treatment

- for dynamic polarizabilities and hyperpolarizabilities of infinite periodic systems. I. Coupled perturbed Hartree–Fock theory. *J. Chem. Phys* **2000**, *113*, 1294–1309.
- (55) Ferrero, M.; Rérat, M.; Orlando, R.; Dovesi, R. The calculation of static polarizabilities of 1-3D periodic compounds. the implementation in the crystal code. *J. Comput. Chem.* **2008**, *29*, 1450–1459.
- (56) Grimme, S.; Hansen, A. A Practicable Real-Space Measure and Visualization of Static Electron-Correlation Effects. *Angew. Chem. Int. Ed.* **2015**, *54*, 12308–12313.
- (57) Bauer, C. A.; Hansen, A.; Grimme, S. The Fractional Occupation Number Weighted Density as a Versatile Analysis Tool for Molecules with a Complicated Electronic Structure. *Chem. Eur. J.* **2017**, *23*, 6150–6164.
- (58) Bialas, D.; Zhong, C.; Würthner, F.; Spano, F. C. Essential states model for merocyanine dye stacks: bridging electronic and optical absorption properties. *J. Phys. Chem. C* **2019**, *123*, 18654–18664.
- (59) Arjona-Esteban, A.; Krumrain, J.; Liess, A.; Stolte, M.; Huang, L.; Schmidt, D.; Stepanenko, V.; Gsa, M.; Hertel, D.; Meerholz, K. et al. Influence of Solid-State Packing of Dipolar Merocyanine Dyes on Transistor and Solar Cell Performances. *J. Am. Chem. Soc.* **2015**, *137*, 13524–13534.
- (60) Hoche, J.; Schulz, A.; Lysanne, B.; Dietrich, M.; Humeniuk, A.; Stolte, M.; Schmidt, D.; Brixner, T.; Frank, A.; Mitric, R. The origin of the solvent dependence of fluorescence quantum yields in dipolar merocyanine dyes . *Chemical Science* **2019**,
- (61) Gildemeister, N.; Ricci, G.; Böhner, L.; Neudörfl, J. M.; Hertel, D.; Würthner, F.; Negri, F.; Meerholz, K.; Fazzi, D. Understanding the structural and charge transport property relationships for a variety of merocyanine single-crystals: a bottom up computational investigation. *J. Mater. Chem. C* **2021**, *9*, 10851–10864.

- (62) Fu, L.; Yaschenko, E.; Resca, L.; Resta, R. Hartree-Fock approach to macroscopic polarization: Dielectric constant and dynamical charges of KNbO₃. *Phys. Rev. B* **1998**, *57*, 6967–6971.
- (63) Djurovich, P. I.; Mayo, E. I.; Forrest, S. R.; Thompson, M. E. Measurement of the lowest unoccupied molecular orbital energies of molecular organic semiconductors. *Org. Electron.* **2009**, *10*, 515–520.
- (64) Tadayyon, S.; Grandin, H.; Griffiths, K.; Coatsworth, L.; Norton, P.; Aziz, H.; Popovic, Z. Reliable and reproducible determination of work function and ionization potentials of layers and surfaces relevant to organic light emitting diodes. *Org. Electron.* **2004**, *5*, 199–205.
- (65) Jacquemin, D.; Perpète, E. A.; Scalmani, G.; Frisch, M. J.; Kobayashi, R.; Adamo, C. Assessment of the efficiency of long-range corrected functionals for some properties of large compounds. *J. Chem. Phys.* **2007**, *126*, 84106.
- (66) Goerigk, L.; Casanova-Paéz, M. The Trip to the Density Functional Theory Zoo Continues: Making a Case for Time-Dependent Double Hybrids for Excited-State Problems. *Aust. J. Chem.* **2021**, *74*, 3–15.
- (67) Santoro, F.; Jacquemin, D. Going beyond the vertical approximation with time-dependent density functional theory. 2016.
- (68) Wigner, E. On the Quantum Correction For Thermodynamic Equilibrium. *Phys. Rev.* **1932**, 749–759.
- (69) Fang, C.; Oruganti, B.; Durbeej, B. How method-dependent are calculated differences between vertical, adiabatic, and 0-0 excitation energies? *J. Chem. Phys. A* **2014**, *118*, 4157–4171.

- (70) Georg, H. C.; Coutinho, K.; Canuto, S. Solvent effects on the UV-visible absorption spectrum of benzophenone in water: A combined Monte Carlo quantum mechanics study including solute polarization. *J. Chem. Phys.* **2007**, *126*, 700.
- (71) Coutinho, K.; Canuto, S. Solvent effects in emission spectroscopy: A Monte Carlo quantum mechanics study of the $n \leftarrow \pi^*$ shift of formaldehyde in water. *J. Chem. Phys.* **2000**, *113*, 9132.
- (72) Grimme, S. Semiempirical hybrid density functional with perturbative second-order correlation. *J. Chem. Phys.* **2006**, *124*, 34108.
- (73) Send, R.; Valsson, O.; Filippi, C. Electronic Excitations of Simple Cyanine Dyes: Reconciling Density Functional and Wave Function Methods. *J. Chem. Theory Comput.* **2011**, *7*, 444–455.
- (74) Boulanger, P.; Jacquemin, D.; Duchemin, I.; Blase, X. Fast and accurate electronic excitations in cyanines with the many-body bethe-salpeter approach. *J. Chem. Theory Comput.* **2014**, *10*, 1212–1218.
- (75) Faber, C.; Boulanger, P.; Attaccalite, C.; Duchemin, I.; Blase, X. Excited states properties of organic molecules: From density functional theory to the GW and Bethe-Salpeter Green’s function formalisms. *Philos. Trans., Math. Phys. Eng. Sci.* **2014**, *372*.
- (76) Kresse, G.; Hafner, J. Ab Initio Molecular Dynamics for Liquid Metals. *Phys. Rev. B* **1993**, *47*, 558–561.
- (77) Kresse, G.; Furthmüller, J. Efficiency of Ab-initio Total Energy Calculations for Metals and Semiconductors Using a Plane-wave Basis Set. *Comput. Mater. Sci.* **1996**, *6*, 15–50.
- (78) Kresse, G.; Hafner, J. Norm-conserving and Ultrasoft Pseudopotentials for First-row and Transition Elements. *J. Phys. Condens. Matter* **1994**, *6*, 8245–8257.

- (79) Hestand, N. J.; Spano, F. C. Expanded Theory of H- and J-Molecular Aggregates: The Effects of Vibronic Coupling and Intermolecular Charge Transfer. *Chem. Rev.* **2018**, *118*, 7069–7163.
- (80) Liess, A.; Arjona-Esteban, A.; Kudzus, A.; Albert, J.; Krause, A. M.; Lv, A.; Stolte, M.; Meerholz, K.; Würthner, F. Ultranarrow Bandwidth Organic Photodiodes by Exchange Narrowing in Merocyanine H- and J-Aggregate Excitonic Systems. *Adv. Funct. Mater.* **2019**, *29*, 1–9.
- (81) Zitzler-Kunkel, A.; Lenze, M. R.; Kronenberg, N. M.; Krause, A. M.; Stolte, M.; Meerholz, K.; Würthner, F. NIR-absorbing merocyanine dyes for BHJ solar cells. *Chem. Mater.* **2014**, *26*, 4856–4866.

Supporting Information Available

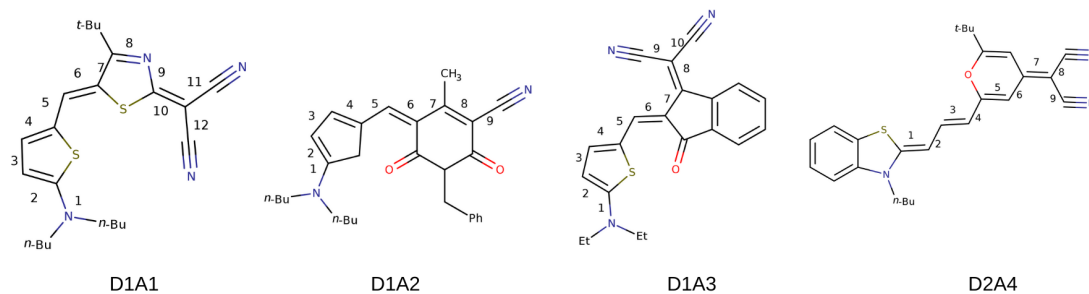
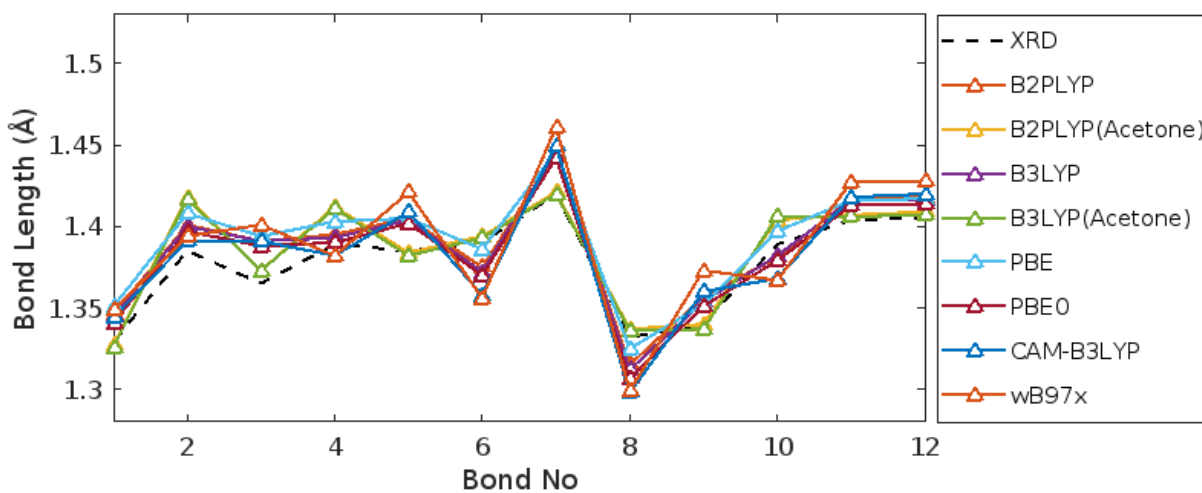
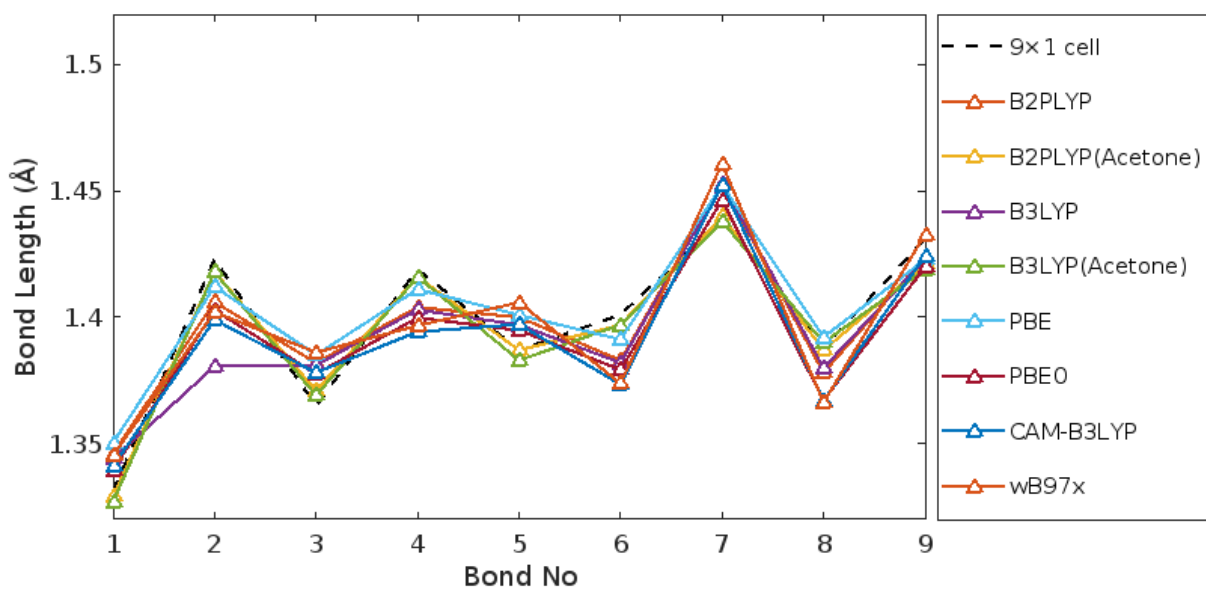
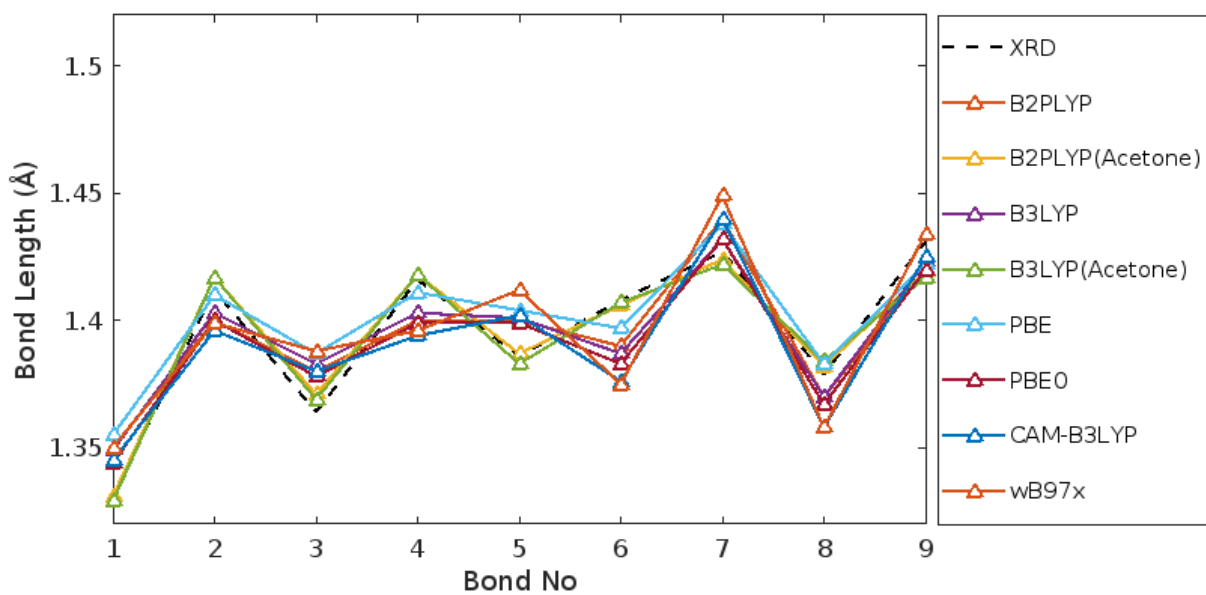


Figure S1: Bond Length alternation paths for merocyanine.





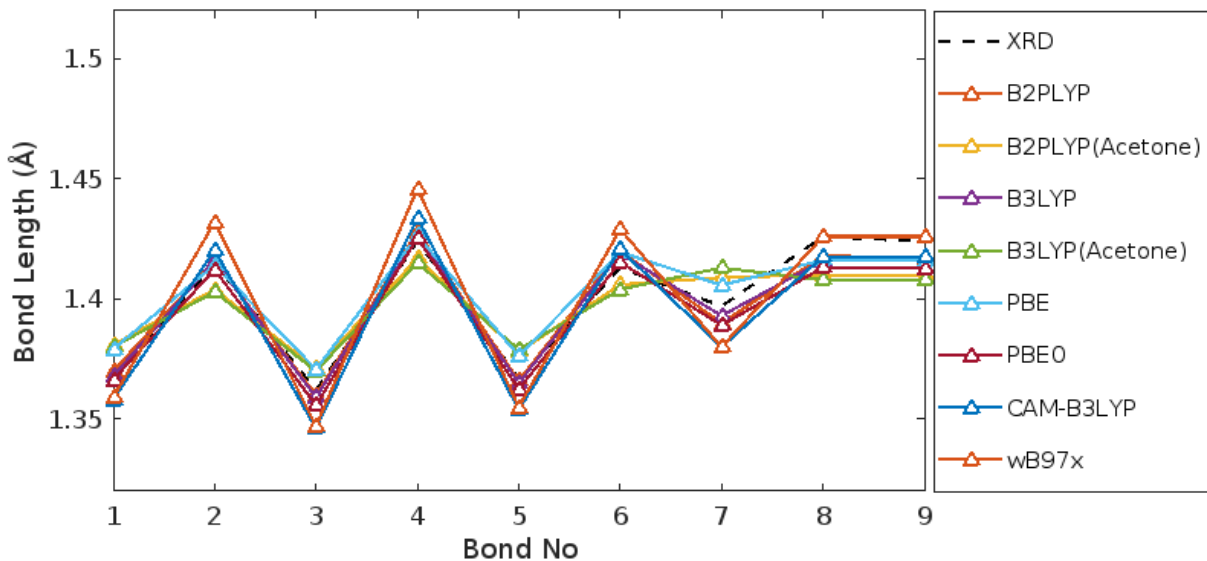


Figure S2: Comparison of the calculated and measured bond length alternations of the merocyanines investigated in this work, namely D1A1, D1A2, D1A3 and D2A4 using B2PLYP, B3LYP, PBE, PBE0, CAM-B3LYP and wB97x for gas phase optimizations and B2PLYP and B3LYP for solvent (acetone) optimizations.

Table S1: Basis-set dependence of the vertical transition energy (eV) of D1A1 calculated with different functionals

Functionals	$S_0 - S_1$ (eV)		
	TZVP	TZVPP	QVZPP
PBE	2.75	2.75	2.74
PBE0	2.87	2.87	2.86
B3LYP	2.84	2.84	2.83
CAM-B3LYP	2.91	2.91	2.90

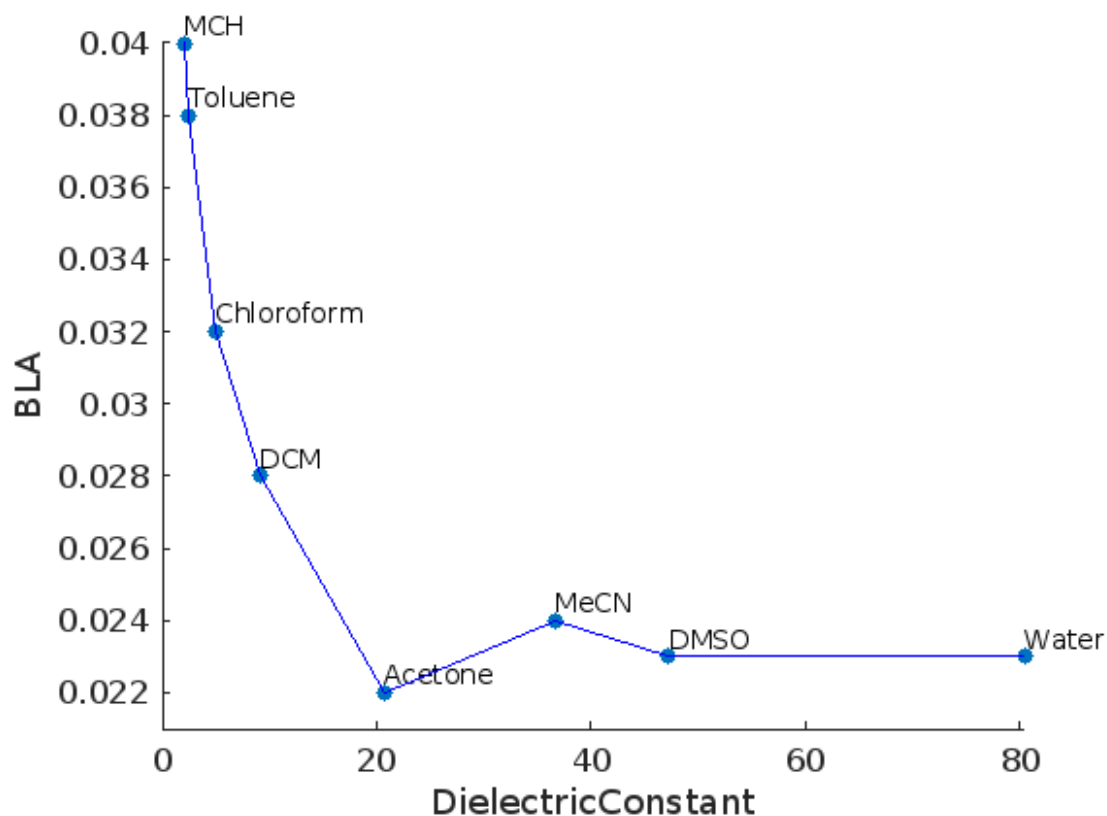


Figure S3: The bond length alternation dependence of MC D2A4 on the dielectric constant of the solution calculated at B2PLYP/D3 level with def2-TZVP basis set. Actual values are represented by circles, solid line serve as guide to the eye.

Table S2: Basis-set dependence of the HOMO energy (eV) of D1A1 calculated with different functionals

Functionals	HOMO(eV)					
	cc-pVDZ			cc-pVTZ		
	G ₀ W ₀	G ₆ W ₀	G ₆ W ₆	G ₀ W ₀	G ₆ W ₀	G ₆ W ₆
PBE	-5.70	-5.79	-5.99	-6.19	-6.38	-6.56
B3LYP	-5.97	-5.97	-6.11	-6.48	-6.55	-6.68
BHLYP	-6.31	-6.28	-6.33	-6.79	-6.81	-6.67

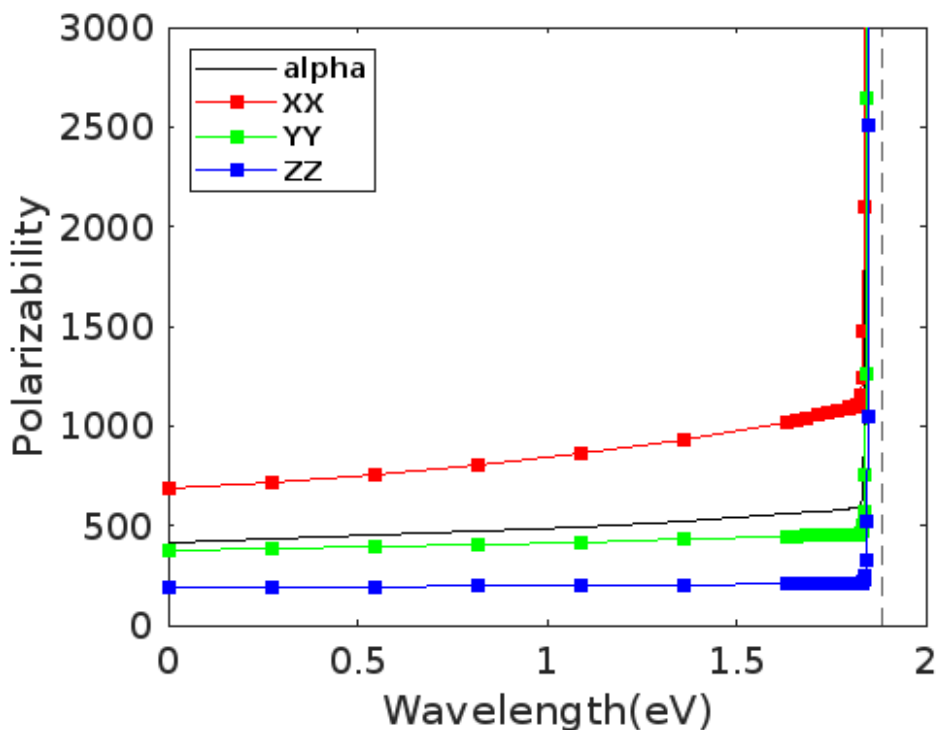


Figure S4: The energy dependence of the many-body polarizability tensor for **D1A1** merocyanine molecule in gas phase computed using TDCP-B3LYP. Actual values are represented by squares, dashed lines serve as visual cues. The dashed lines represent the optical gap of the molecule.

Table S3: Crystallographic Parameters of MCs including the two different polymorphs of D1A1 namely P1 and P2.

	P1-D1A1 ^a	P2-D1A1 ^b	D1A2 ^c	D1A3 ^d	D2A4 ^e
Temp. (K)	295	100	100	100	100
CCDC	2073437	2073438	1007699	1406539	1957268
a(Å)	13.09	13.94	8.17	4.96	7.03
b(Å)	19.3	18.85	11.65	13.74	11.04
c(Å)	9.84	9.08	13.66	26.02	15.22
$\alpha(^{\circ})$	90	90	107.7	90	76.5
$\beta(^{\circ})$	101.7	105.6	102.1	93.3	89.7
$\gamma(^{\circ})$	90	90	96.2	90	78.3
Z	4	4	2	4	2
Space Group	<i>P</i> 21/ <i>c</i>	<i>P</i> 21/ <i>c</i>	<i>P</i> – 1	<i>P</i> 21/ <i>n</i>	<i>P</i> – 1

^a:Reference⁶¹; ^b:Reference⁶¹; ^c:Reference⁸¹; ^d:Reference⁵⁹; ^e:Reference⁶⁰;

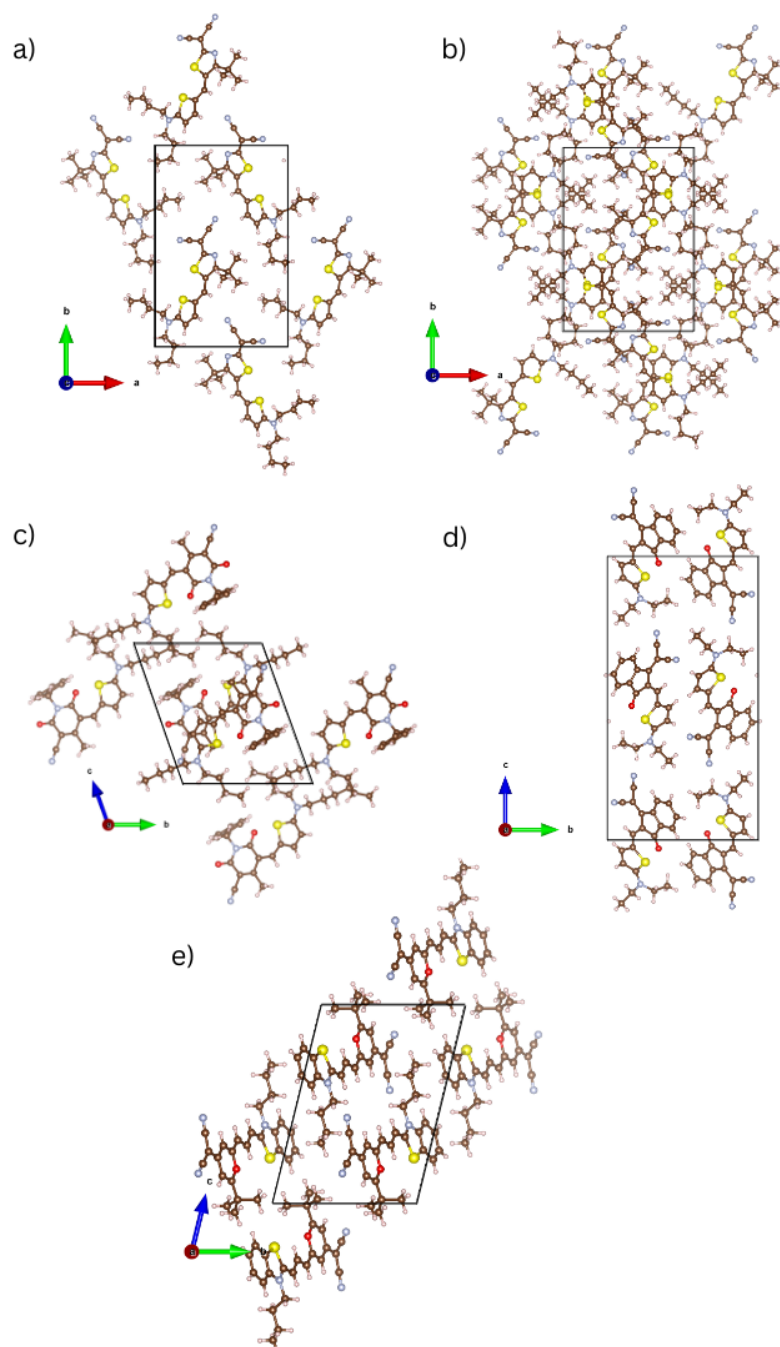


Figure S5: The molecular crystal structures of D1A1 polymorphs a) P1-D1A1, b)P2-D1A1 and merocyanines c) D1A2, d) D1A3 and d) D2A4.

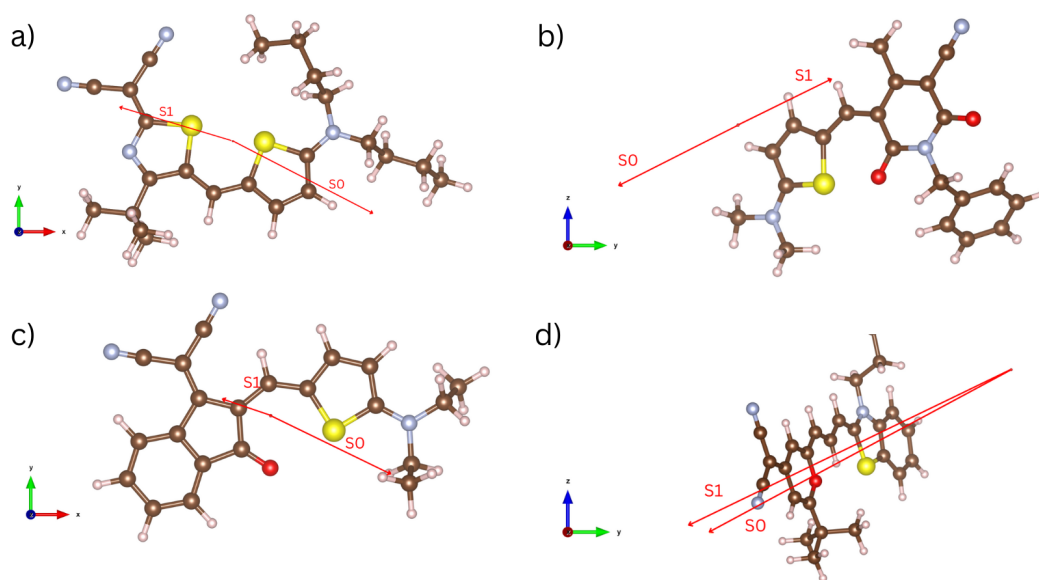


Figure S6: Transition dipole moment vectors for the ground state (S_0) and first excited state (S_1) calculated using TD-DFT at PBE-D3/def2-TZVPP level of merocyanines: a) D1A1, b) D1A2, c) D1A3 and d) D2A4.

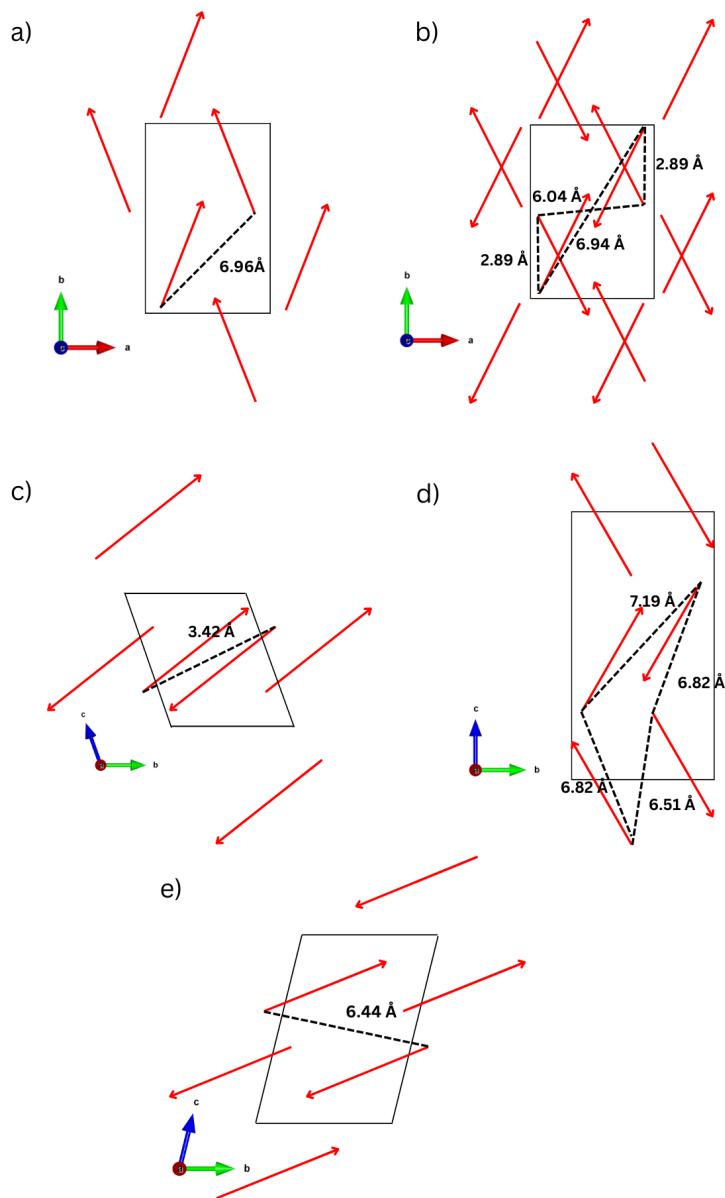


Figure S7: Representative picture of the excited state transition dipole moment for the crystal structures given in Figure S4. The red arrows represent the direction of transition dipole moment vectors of each molecular unit the crystal structure of the respective merocyanines and the black dotted lines represent the distance between the barycentre of adjacent molecules.

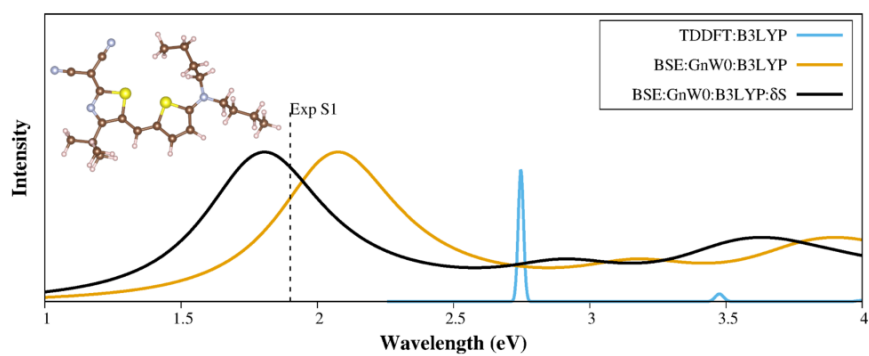


Figure 8: Graphical abstract